Geochemistry, Geophysics, Geosystems

RESEARCH ARTICLE
10.1029/2020GC008917

Hydrothermal Chimney Distribution on the Endeavour Segment, Juan de Fuca Ridge

David A. Clague[1], Julie F. Martin[2], Jennifer B. Paduan[1], David A. Butterfield[3], John W. Jamieson[4], Morgane Le Saout[1,5], David W. Caress[1], Hans Thomas[1], James F. Holden[6], and Deborah S. Kelley[7]

[1]Monterey Bay Aquarium Research Institute, Moss Landing, CA, USA, [2]School of Natural Sciences, California State University at Monterey Bay, Marina, CA, USA, [3]JISAO, University of Washington and Pacific Environmental Laboratory, Seattle, WA, USA, [4]Department of Earth Sciences, Memorial University of Newfoundland, St. John's, Newfoundland, Canada, [5]Now at Department of Magmatic and Hydrothermal Systems, GEOMAR, Helmholtz Centre for Ocean Research, Kiel, Germany, [6]Department of Microbiology, University of Massachusetts, Amherst, MA, USA, [7]School of Oceanography, University of Washington, Seattle, WA, USA

Key Points:
- The Endeavour Segment of the Juan de Fuca Ridge hosts 572 hydrothermal sulfide chimneys in the central 14 km of the segment
- Hydrothermal activity is limited to the axial graben and the near rims of the graben above the seismically imaged magma lens
- The minimal eruptive activity on Endeavour for the past 4,300 years does not bury inactive chimneys as occurs on other ridges

Supporting Information:
- Supporting Information S1
- Table S1
- Figure S1

Correspondence to:
D. A. Clague,
clague@mbari.org

Citation:
Clague, D. A., Martin, J. F., Paduan, J. B., Butterfield, D. A., Jamieson, J. W., Le Saout, M., et al. (2020). Hydrothermal chimney distribution on the Endeavour Segment, Juan de Fuca Ridge. *Geochemistry, Geophysics, Geosystems*, *21*, e2020GC008917. https://doi.org/10.1029/2020GC008917

Received 13 JAN 2020
Accepted 9 APR 2020
Accepted article online 14 APR 2020

Abstract The Endeavour Segment of the Juan de Fuca Ridge is well known for its abundance of hydrothermal vents and chimneys. One-meter scale multibeam mapping data collected by an autonomous undersea vehicle revealed 572 chimneys along the central 14 km of the segment, although only 47 are named and known to be active. Hydrothermal deposits are restricted to the axial graben and the near-rims of the graben above a seismically mapped axial magma lens. The sparse eruptive activity on the segment during the last 4,300 years has not buried inactive chimneys, as occurs at more magmatically robust mid-ocean ridges.

1. Introduction

The Endeavour Segment of the Juan de Fuca Ridge, hereafter referred to simply as Endeavour, is unusual for its widespread hydrothermal venting that has produced abundant large sulfide chimneys in a setting characterized by low volcanic output and intense tectonism (e.g., Delaney et al., 1992; Glickson et al., 2007; Karsten et al., 1986; Karsten et al., 1990; Kelley et al., 2012; Robigou et al., 1993). The segment was specified as a RIDGE 2000 Program Integrated Study Site and later was selected as the site for a node of the cabled observatory operated by NEPTUNE Canada (Kelley et al., 2014). It has been the site of numerous hydrothermal, biological, geological, and geophysical studies (e.g., Delaney et al., 1992; Kelley et al., 2002; Kelley et al., 2012) dating back to the 1980s.

More recently completed 1-m resolution mapping, combined with minimum ages of lava flows, indicates that the axial graben began to form during a tectonic phase that started ~4,300 years ago (Clague et al., 2014). The subsequent hydrothermal phase began inside the widening axial graben ~2,300 years ago as defined by ages of sulfide deposits (Jamieson et al., 2013) and minimum ages of lava flows within the axial graben (Clague et al., 2014). The hydrothermal phase, Clague et al.'s (2014) addition to the Kappel and Ryan (1986) model of tectonic-magmatic cycles, continues today. The 1-m resolution mapping data, which resolve individual chimney structures, were used to determine the volume and tonnage of the extensive hydrothermal deposits (Jamieson et al., 2014). The general distribution of chimneys and chimney fields was recently used to evaluate models of ridge segmentation (Le Saout et al., 2019; VanderBeek et al., 2016).

Here, we describe and discuss the spatial distribution of the mapped hydrothermal chimneys and present maps of the five named vent fields.

2. Geologic Setting

Endeavour is located in the NE Pacific (Figure 1). The segment is bounded to the south by the Cobb Propagator at the northern end of the Northern Symmetrical Segment. At the north end, Endeavour overlaps with the West Valley Segment. Endeavour has an intermediate full-spreading rate of 57 mm/year (DeMets et al., 2010), and a 1.2–1.7 km wide axial graben. The segment has experienced intense seismic swarms related to dike intrusions (Weekly et al., 2013) that perturbed the hydrothermal system (Hooft et al., 2010;

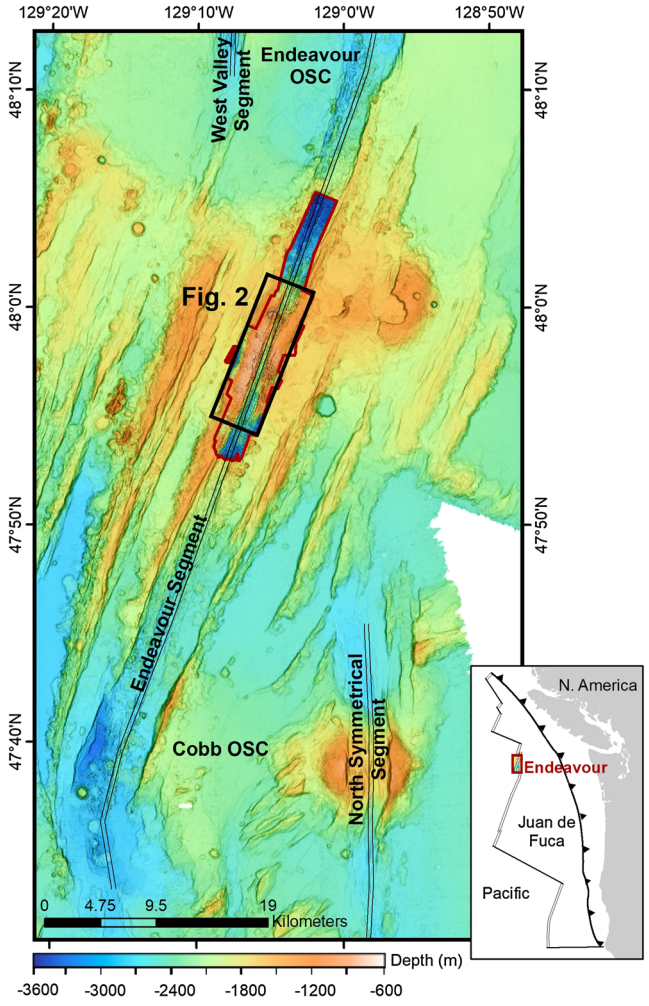

Figure 1. Map showing the Endeavour Ridge. Bathymetric data collected by the R/V *Thompson* using Simrad EM300 and Simrad EM302 systems, gridded at 50 m resolution. Spreading segments and tectonic plate boundaries are shown, and OSC indicates overlapping spreading center. The red outline shows the combined extent of the MBARI AUV and ABE bathymetry data (Clague et al., 2014). The black box shows extent of AUV data shown in Figure 2.

Kelley et al., 2002; Kelley et al., 2012; Lilley et al., 2003) consistent with well-established relations between magmatism, tectonism, and hydrothermalism on ridges (Perfit & Chadwick, 1998). Clague et al. (2014) describe the volcanology and structure for the complete high-resolution AUV map, and Le Saout et al. (2019) define four subsegments (Figure 2b) with AV1 in the south along the west margin of the axial graben, AV2a extending northward from Mothra through Main Endeavour Field (MEF) and High Rise, ending at Cirque and Dune vents (Figure 2b). Most of subsegment AV2a is close to the center of the axial graben. Subsegment AV2b extends north from Vesta vent through the Salty Dawg and Sasquatch vent fields along the eastern side of the axial graben. The fourth and most northerly subsegment, AV3, is northwest of the northern end of AV2b but does not have any identified chimneys.

Endeavour has abundant and vigorous hydrothermal activity concentrated in the axial graben (e.g., Kelley et al., 2012). This activity has produced some of the tallest and most voluminous hydrothermal chimneys known from the mid-ocean ridge system (Delaney et al., 1992; Kelley et al., 2002; Robigou et al., 1993). The two southernmost active vent fields, Mothra and MEF, are instrumented as part of the NEPTUNE Canada cabled observatory (Barnes et al., 2011; Kelley et al., 2014). Much, but not all, of the active venting is localized in the five main hydrothermal vent fields including the two instrumented fields and the more northern High Rise, Salty Dawg, and Sasquatch fields (e.g., Delaney et al., 1992; Delaney et al., 1997; Glickson et al., 2006, 2007; Kelley et al., 2001; Kelley et al., 2002; Kelley et al., 2012; Robigou et al., 1993). Together, the main five active fields and an area surrounding them are designated a Canadian Marine Protected Area bounded by 47°54′N, 48°01′N, 129°2′W, and 129°8′W. Despite three decades of study at these active vent fields, a comprehensive map of the distribution of hydrothermal chimneys has not been published. The volume and tonnage of the sulfide deposits (Jamieson et al., 2014) were estimated using the same data set presented here.

3. Collection and Processing of High-Resolution Multibeam Data

The primary bathymetric data for this study were collected using the MBARI AUV *D. Allan B.*, a Dorado class vehicle (Caress et al., 2008; Paduan et al., 2009) outfitted with a Reson 7125 200 kHz multibeam sonar that produced soundings with 0.82- and 1.67-m wide beam footprints, at nadir and 45°, respectively, with 0.1-m vertical resolution for the 50-m altitude surveys. The lateral resolution is therefore ~1.25 m. A map of MEF is shown in Figure S1C in the supporting information, and an oblique view of the vent field is presented in Figure S1D. Details of the navigation and sensors on the AUV *D. Allan B.* are in Clague et al. (2014) for the surveys at Endeavour. The *D. Allan B.* executed four 10–11.5-hr surveys during the R/V *Atlantis* cruise AT1536 in 2008 and three additional 17.5-hr surveys in August 2011 from the R/V *Zephyr*.

High-resolution multibeam data were collected in 2005 by the University of Washington using the Woods Hole Oceanographic Institution's AUV *ABE*, equipped with a Simrad Mesotech SM2000 multibeam sonar (Kelley et al., 2012). ABE completed nine missions at Endeavour; results from six of them are presented in Clague et al. (2014). The ABE surveys generally produced maps with resolution of 3.92 m at nadir and 8.07 m at 45° for surveys done at 150-m altitude, as shown in Figure S1A, which is gridded at 5 m. One survey at the MEF was executed at 45-m altitude with 1.31-m beam footprints at nadir and 2.67 m at 45° and yielded a map with ~2 m average lateral resolution (Figure S1B and perspective images in Kelley et al., 2012).

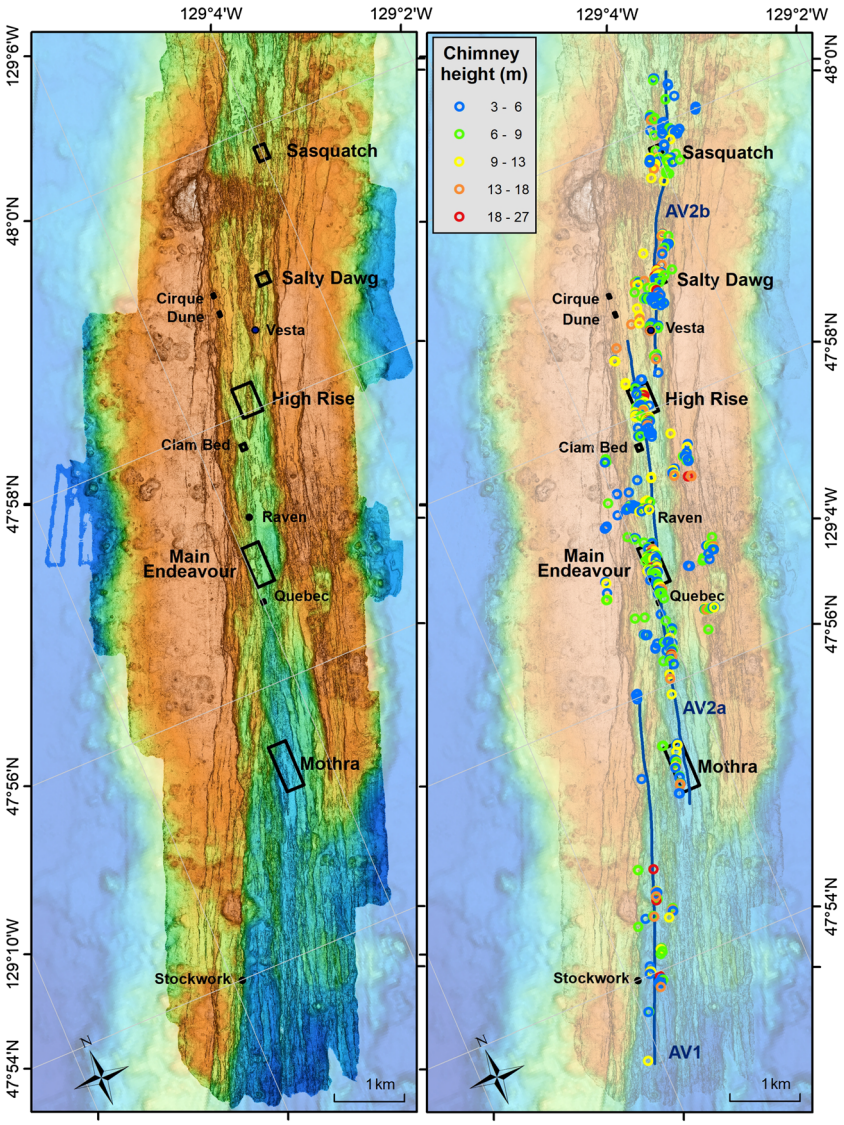

Figure 2. (a). MBARI *D. Allan B.* AUV bathymetric data gridded at 1 m, over *ABE* data gridded at 5 m, over faded Simrad data gridded at 25 m. The map is rotated 23° from north and is in UTM zone 9N, and the depth range is −2,550 (dark blue) to −1,940 m (orange). Black boxes outline the extents of the previously named active vent fields (Glickson et al., 2007), Sasquatch, Salty Dawg, High Rise, Main Endeavour, and Mothra, and small black circles show smaller active vent fields named Cirque, Dune, Vesta, Clambed, Raven, Quebec, and Stockwork (Kelley et al., 2012). Each of the main active vent fields is shown in more detail in Figure 3. (b). Faded AUV multibeam bathymetry. Circles mark the chimney locations identified from the AUV data; colors indicate chimney height determined from the AUV data. Blue lines labeled AV1, AV2a, and AV2b are segment axes from Le Saout et al. (2019).

To maximize coverage, we planned overlap between swaths at about 30 m, which still resulted in some gaps between adjacent lines in this rough terrain. The navigation adjustments were aided by crossing lines. The area surveyed is about 62 km^2 of nearly complete mapping coverage including the entire floor of the axial graben for 23.8 km from 47°53.05′N to 48°5.13′N and between 2.0 and 5.0 km wide. The combined *ABE* and *D. Allan B.* surveys cover an area of 71.7 km^2.

The *D. Allan B.* multibeam data were processed using the MB-System software package (Caress & Chayes, 1996, 2011). The navigation was adjusted to match features in overlapping swaths using the MB-System tool MBnavadjust, resulting in a navigation model with relative accuracy equivalent to the 1.25-m lateral resolution. The AUV bathymetry was also matched to GPS-navigated, hull-mounted Simrad

EM302 multibeam bathymetry collected from the R/V *Thompson*, resulting in an absolute position accuracy on the order of ~20 m. Specific features in the high-resolution map data can be colocated with the same features observed during ROV dives navigated using ultrashort baseline or long baseline.

The *ABE* data were coregistered with subsequently collected MBARI AUV data by converting the EM2000 sonar swath files to mb71 files, manually editing the data using MBedit in MB-System, adjusting horizontal and vertical offsets for matching of features within the ABE surveys and matching to overlapping MBARI AUV data using the MBnavadjust tool in MB-System.

4. Identification of Chimney Structures

The grids were manually searched for positive anomalies that we interpret as sulfide chimneys, and in most cases, we examined the original swath data again to eliminate data artifacts from the compilation. The *ABE* data collected at 150-m altitude are not of high enough resolution to detect most chimneys, and the 45-m altitude *ABE* survey of the MEF was remapped using the *D. Allan B.* at comparable resolution and with better navigation, so only the *D. Allan B.* bathymetry was used to locate chimney structures.

The minimum height of chimneys identified in the grids was limited to 3 m, as below this height there are data artifacts and nonhydrothermal structures. Primary among these structures are lava pillars (Ballard et al., 1979; Fundis et al., 2010) that form near the margins of drained ponded channelized flows. Several such "pillars" rise above the apparent shallowest flow surface and were included in our preliminary inventory of chimneys. Most, however, define the precollapse roof of a flow and were eliminated from the compilation, although a few in faulted terrain may remain. Other small steep anomalies that are not chimneys are located at the tops of pillow mounds, where the last few pillows make small mounds several meters tall. Clague and Paduan (2009) describe many submarine volcanic features as mapped by various underwater vehicles with sonars of different resolution, including the MBARI AUV, and some of our interpretation here depends on combined mapping and dive observations made elsewhere. There are also artifacts in the data that can appear chimney-like but can usually be identified by examination of the cloud of data points using the 3-D data editing program MBeditviz.

The combined surveys (Figure 2) superpose a *D. Allan B.* 1.25-m grid on an *ABE* 5 m grid and then superpose both on a regional Simrad EM302 multibeam bathymetry 25 m grid. The extent of the map is limited to the northernmost and southernmost detected chimney structures. The chimneys identified using this same data set by Jamieson et al. (2014) were all reexamined to improve reliability based on lessons learned at Alarcon Rise in the Gulf of California (Paduan et al., 2018) where almost all identified chimneys were visually observed during ROV dives. We removed 193 apparent, but spurious, chimneys and added 27 new ones to the initial inventory of 766 chimneys. Most of the chimneys removed from the inventory were close to our cutoff anomaly height of 3 m and so reduce the estimated volume of sulfide deposits on the Endeavour Segment by no more than perhaps 10% (Jamieson et al., 2013). Jamieson et al. (2013) also combined chimneys if the mounds surrounding them merged.

The 1.25-m resolution data allow identification of individual hydrothermal chimneys and estimation of their height above the surrounding terrain (Figure 2b). The map shows 572 chimney structures (Figure 2), of which 47 (8.2%) are known to be active, previously known, and named (e.g., Delaney et al., 1992; Glickson et al., 2007; Kelley et al., 2012; Robigou et al., 1993). Numerous other mapped chimneys have been observed to be inactive during submersible and ROV dives, but coregistering the observations to the features in the maps is hampered by navigational uncertainties. The number of individual chimneys is different from the list of deposits in supplemental material in Jamieson et al. (2014) because the deposits commonly include more than a single chimney structure and because structures previously identified as chimneys (Clague et al., 2008) are now recognized as noise in the sonar data or as small horsts. About 87% of the identified chimneys are located along ~14.5 km of the axial graben centered on the inflated part of the ~95-km long Endeavour segment, with the remaining 13% divided between 18 and 55 chimneys on the west and east flanks of the segment, respectively. The northernmost mapped chimney is located ~41 km south of the northern end of the segment and the southernmost mapped chimney is located ~39 km north of the south end of the segment. All the hydrothermal chimneys are therefore located in the central ~15% of the segment, and the known active chimneys and vents occur along the central ~9% of the segment. The chimneys outside the axial graben stretch for ~2.1 and 2.8 km parallel to the axis on the west and east flanks, respectively, with

both between Quebec and Clam Beds vents (Figure 2b). The most distal chimneys occur 795 m east and 760 m west of the AV2a axis near the central part of the segment. Flank chimneys near the north end of the known chimneys are within 420 and 290 m east and west of the AV2b axis, and those near the southern end are within 220 and 230 m east and west of AV1 axis.

Some well-known vents that are routinely sampled for water chemistry or microbes (see summary in Kelley et al., 2012) are too small to be seen in the maps, so the number of chimneys indicated is a minimum estimate of active vents and formerly active vents. Figure 2 also shows the locations of the five named active hydrothermal vent fields as boxes—Mothra, MEF, High Rise, Salty Dawg, and Sasquatch—(Figure 1c in Glickson et al., 2007), and some additional named sites (Kelley et al., 2012) are identified. These five vent fields stretch along 8.8 km of the axial graben. Many of the chimney structures are located outside the five primary active vent fields, but the density of chimneys is highest at High Rise and MEF.

The detailed bathymetry for each of five main named vent fields is shown in Figure 3. The left-hand images present the mapping data unobscured by chimney names, contours, or chimney height determined from the AUV data (color-coded), which are added to the right-hand figures. At the three northern vent fields, chimneys occur in nearly equal abundance outside the defined active vent fields as within. Even at the relatively large MEF and Mothra vent fields, numerous chimneys occur outside the active vent fields.

We will first describe the mapping results in the vicinity of the five primary vent fields, in order from north to south, and then describe some of the chimneys and hydrothermal mounds located outside these fields.

4.1. Mothra

The Mothra vent field chimneys (Figure 3a) are spread over about 150 m of the axial graben, mainly on its western side along the southern portion of subsegment AV2a (Le Saout et al., 2019). As at all the named vent fields, chimneys occur well outside the boundaries that defined the vent fields (Glickson et al., 2007; Kelley et al., 2001). Chimneys are abundant south of Mothra field, both in the axial graben and along the faulted northwestern graben wall.

4.2. MEF

The field including 53 mapped chimneys is located along the base of the faults bounding the northwest side of the axial graben (Figure 3b). Seventeen vents are named and some are instrumented with monitoring sensors (Delaney et al., 1992, 1997; Neptune Cabled Observatory; Kelley et al., 2014). Chimneys at several of the named vents at MEF are too small to be distinguished in the AUV data. An active vent named Raven is located north of MEF, and another active vent named Quebec is located south of MEF (Figure 2b). Many inactive chimneys are known to the east and southeast of the active MEF vents. The MEF is located along the central part of subsegment AV2a (Le Saout et al., 2019).

4.3. High Rise

The High Rise vent field (Figure 3c) is aligned along a steep horst block of lavas that is oriented parallel to the ridge axis (Robigou et al., 1993) and defines the axis of subsegment AV2a (Le Saout et al., 2019). Many of the chimneys here are tall, and nine have been named, including Godzilla, which was measured at 45 m tall prior to its collapse in 1995 (Robigou et al., 1993; Robigou et al., 1995). The chimneys are abundant along most of the 1.5 km-long horst, concentrated on the east side at the southern end and the west side at the northern end. Common smaller chimneys dot the lower-relief flows and ridges NW of the main vent field. The smooth, faulted channelized flows east of the horst lack chimneys. To the southwest of High Rise, a vent field named Clam Bed (Kelley et al., 2012) lacks chimneys large enough to detect in the AUV data and is primarily low-temperature diffuse venting.

4.4. Salty Dawg

The Salty Dawg vent field (Figure 4a) contains four named chimneys, including Grendl (which reaches 25 m in height and is ~30 m long) and Beowulf and Salty Dawg, both located close to the northern limit of the box defining the vent field (Delaney et al., 1997; Glickson et al., 2007). Chimneys are distributed along and within 100 m of a ridge axis-parallel volcanic ridge that defines subsegment AV2b (Le Saout et al., 2019) in the area (Figure 2b) and continue south along the ridge to an active vent named Vesta (Figure 2b)

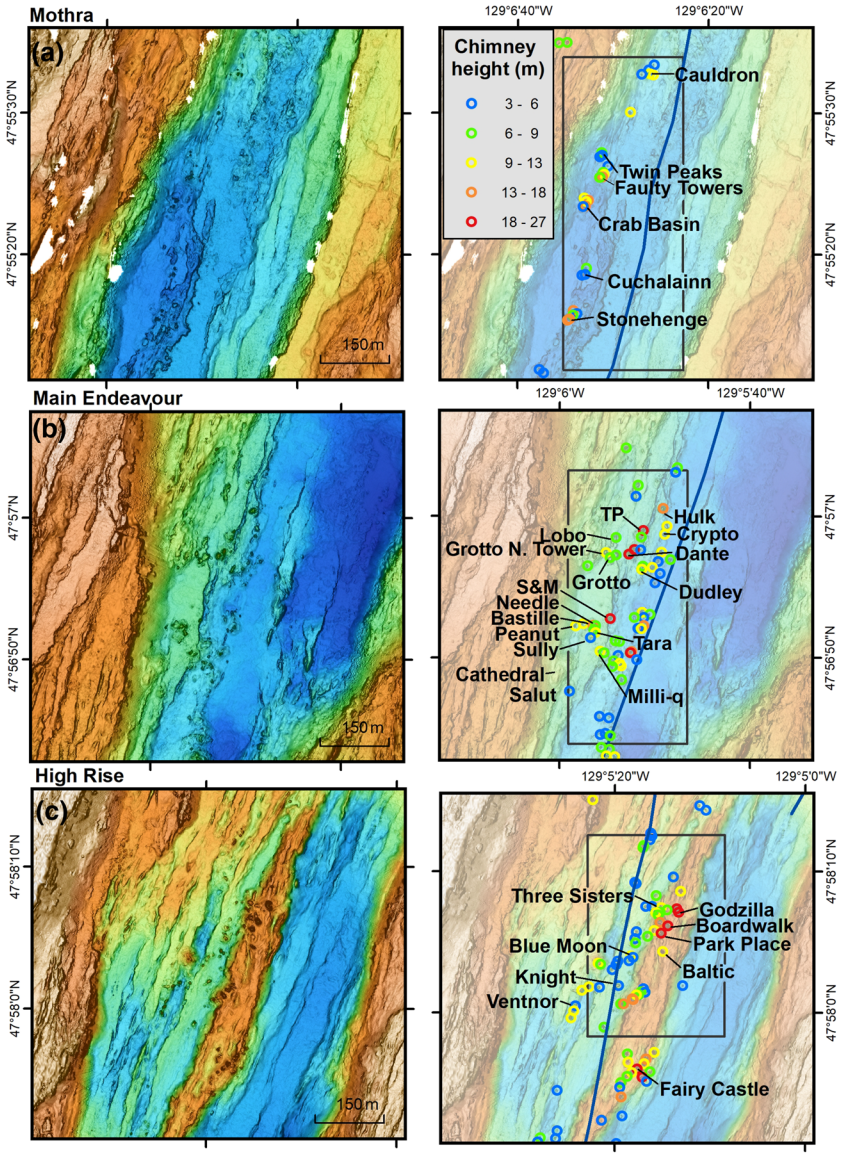

Figure 3. AUV bathymetry maps of the (a) Mothra (b) Main Endeavour, and (c) High Rise active hydrothermal vent fields on Endeavour subsegment AV2a (Le Saout et al., 2019). The right panel shows faded bathymetry with circles marking chimney locations identified from the AUV data; symbol colors indicate chimney height measured from the AUV data. Black boxes outline the extents of the previously named active vent fields (Glickson et al., 2007). Vent names from Robigou et al. (1993), Delaney et al. (1992), and Glickson et al. (2007). All maps are gridded at 1 m and plotted at a scale of 1:10,000. Color scale has been histogram equalized for each map.

Abundant chimneys also occur on the volcanic ridge centered about 500 m west of the Salty Dawg field where vent sites Cirque and Dune are located (Figure 2b) on the northern end of subsegment AV2a (Le Saout et al., 2019).

4.5. Sasquatch

Chimneys are sparsely distributed at the Sasquatch field (Figure 4b), and one named chimney, Pico, may be located ~50 m north of the vent field box defined by Glickson et al. (2007). The chimneys are mainly aligned along a volcanic ridge constructed of pillow lavas that defines subsegment AV2b in the area (Le Saout et al., 2019), although smaller chimneys are scattered among the volcanic ridges and valleys within roughly 800 m to the NE, SW, and E of the named vent field.

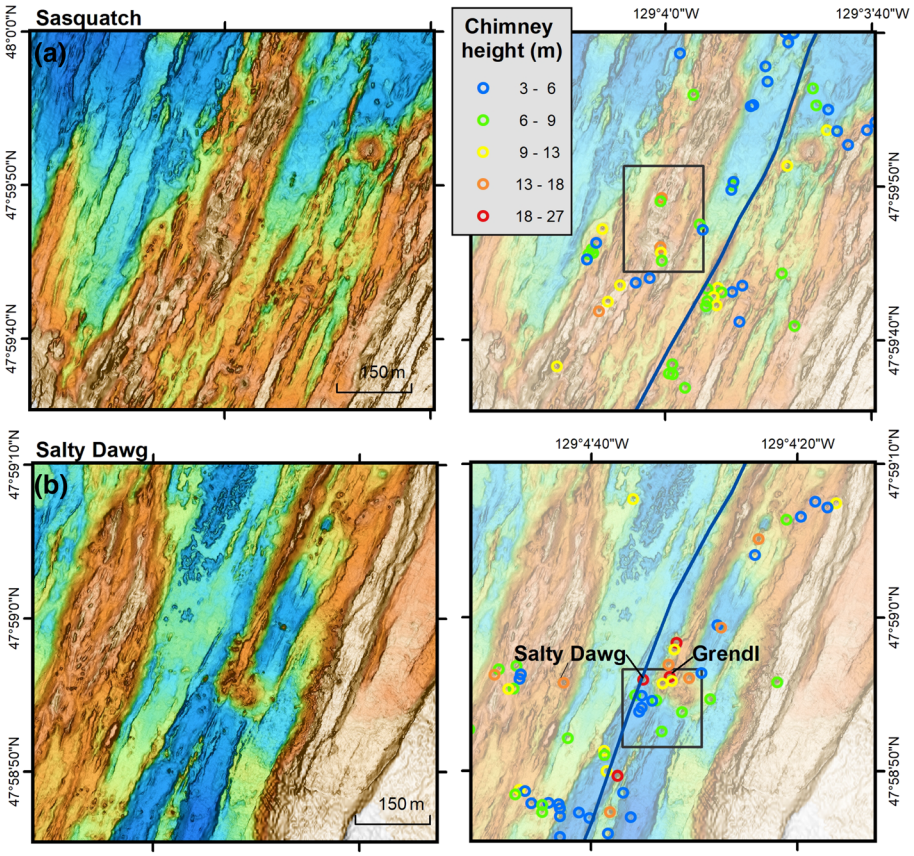

Figure 4. AUV bathymetry maps of the (a) Sasquatch and (b) Salty Dawg active hydrothermal vent fields on Endeavour subsegment AV2b (Le Saout et al., 2019). Details as described in Figure 3.

4.6. Other Chimney Structures and Hydrothermal Mounds

The named vent sites Quebec, Clam Bed, and Dune (Figure 2) have no chimneys evident in the AUV data, consistent with diffuse venting observed during ROV and submersible dives at these sites. Chimneys up to 8 m tall are reported at Stockwork, located along subsegment AV1 ~ 2.5 km southwest of Mothra (Kelley et al., 2012). The site is not evident in the AUV data, perhaps because the tall chimney is located at the base of the steep northwest fault bounding the axial graben and so blends into the scarp. Other known active vents are also not imaged in the AUV mapping data, mainly because some active vents have constructed small chimney structures. Chimneys identified near Dune are at least 140–170 m from the location of the known active vents (Kelley et al., 2012). Cirque is located in a data gap in the AUV bathymetry; the nearest identified chimney is about 75 m to the northeast of the proposed site (Kelley et al., 2012).

Eighty-seven percent of the chimneys are located within the axial valley, although they are not all concentrated in a narrow zone along the axis of the valley. Thirty-five chimneys occur north of the Sasquatch field, and 44 more are located as far as 3.9 km south of the Mothra field (Figure 2). Rare chimneys occur on the west rim of the axial graben. On the east rim of the axial graben, especially east of MEF, there is an area with more extensive mapping coverage outside the axial valley than to either the north or south, and this area contains chimneys. To the south of MEF where the valley broadens, chimneys are scattered throughout the western half of the axial graben, whereas to the north of High Rise, most chimneys are located in the eastern half of the axial graben.

4.7. Size and Distribution of Chimneys

The chimneys range from 3 m (arbitrary lower cutoff) to 27 m tall, as determined from the AUV data, with the tallest being the structure Godzilla, which rose 45 m above the seafloor before it collapsed in 1995 (Robigou et al., 1995). In many cases, especially if the chimneys are narrow near their tops, the sonar

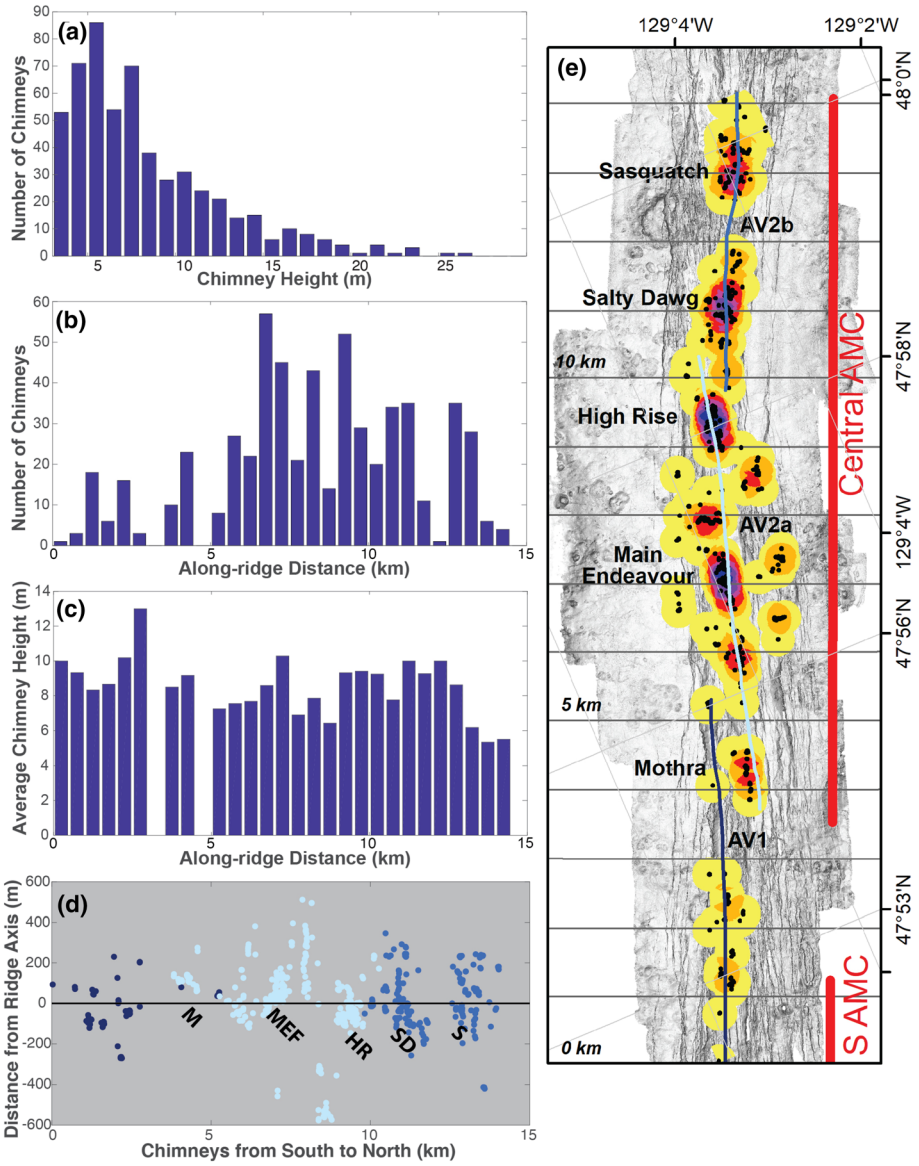

Figure 5. (a) Histogram showing the number of chimneys of different heights, binned in 1-m increments. (b) Histogram showing the total number of chimneys along the Endeavour ridge axis, binned in 0.5-km intervals indicated on Figure 5e. (c) Bar plot showing the distribution of average chimney height along the ridge axis, binned in 0.5-km intervals indicated in Figure 5e. (d) Plot showing the distance (in kilometers) each chimney is offset from the axis of segments AV1, AV2a, and AV2b (Le Saout et al., 2019). M is the Mothra vent field, MEF is the Main Endeavour Field, HR is the High Rise vent field, SD is the Salty Dawg vent field, and S is the Sasquatch vent field. (e) Map shows a density plot of chimneys per square kilometer along the segment with a cell size of 10 m and a neighborhood size of 25 m, with blue and yellow indicating the highest (250–320 chimneys/km^2) and lowest (2–50 chimneys/km^2) chimney densities, respectively. The black dots are the locations of all mapped chimney structures, active and inactive. The overlapping axes of subsegments AV1, AV2a, and AV2b (modified from Le Saout et al., 2019); points in (d) are color-coded to match the closest segments, colors as in (e). The red vertical bars along the right side of the image show the along-axis extents (but not where they lie under the axis) of the central and part of the southern AMC (SAMC) axial magma chambers (AMC) mapped by Van Ark et al. (2007). The northern end of a SAMC is shown, but it extends south beyond the map. A third, less-certain, northern AMC lies entirely north of the map extent. Horizontal lines mark intervals of 1 km; data were binned in 0.5-km intervals in (b) and (c). The area enclosed represents the entire ridge segment represented by the histograms and bar plots.

measurements almost surely underestimated their true heights, so the heights measured should be interpreted as minimum values. A histogram of chimney heights (Figure 5a) shows that there are few chimneys taller than ~15 m and that chimneys have mean and median height of 8.55 ± 4.3 m and 7.0 m.

The chimney-rich part of the axis was divided into 30 equal 0.5-km long sections (Figure 5e) to determine if chimney structures were more abundant (Figure 5b) in certain portions of the axis (where the active vent fields were located, for example). Other than a low abundance at the southernmost part of the mapped axis, the chimneys are widely distributed along axis, with the peak density occurring near MEF, 7 km from the south end of the map. The average chimney height for each 0.5-km long section of the ridge is shown in Figure 5c and shows no significant change in average chimney height from south to north.

The locations of the chimneys are widely scattered but not randomly distributed. The chimney locations and densities are shown projected to the axes of the subsegments (AV1, AV2a, AV2b, and AV3 in Figure 5e) and their distance NW or SE away from these axes is shown in Figure 5d for all measured chimneys. Chimneys for MEF, Salty Dawg, Sasquatch, Mothra, and High Rise are all randomly distributed adjacent to the subsegment axes. Chimneys occur as much as 800 m from subsegment axis AV2b.

4.8. Active Versus Inactive Chimneys

The sonars do not discriminate active from inactive chimneys, although CTD, nephelometer, and E_h data can, if the vehicle intersects with a plume during the programmed 150-m line spacing at an altitude of 50 m (Paduan et al., 2018). The AUV detected temperature anomalies at High Rise and at MEF, and plumes from many known active vents went undetected. Temperature anomalies were detected by the AUV CTD sensor package at two locations far from known active vent fields, and although neither is directly above a mapped chimney, tall chimneys are nearby in both cases. The large number of chimneys mapped relative to the known number of active vents supports the interpretation that most are inactive.

5. Discussion

5.1. What Controls the Distribution of Chimneys and Active Vents?

The abundant chimneys on Endeavour extend from ~47°53.4′N to ~48°00.3′N and closely mimic the along-axis distribution of the axial magma chamber (AMC) (Kelley et al., 2012; Van Ark et al., 2007). This correlation suggests a direct link between the presence of an AMC in the crust and hydrothermal circulation that forms hydrothermal vents and chimneys (Kelley et al., 2012; Van Ark et al., 2007). The correlation is not perfect with the central AMC extending from the northernmost mapped chimney to the south end of the Mothra vent field, but not as far south as chimneys are mapped (Figure 5e). The southern AMC begins near Stockwork but continues south beyond mapped chimneys (Figure 5e). The less certain northern AMC of Van Ark et al. (2007) is located north of all mapped chimneys. Regardless, the main AMC that extends from 47°54.5′N to 48°0.3′N underlies the five active named vent fields, as previously noted (e.g., Van Ark et al., 2007; Kelley et al., 2012; Arnoux et al., 2019). A correlation between magma recharge and hydrothermal heat output (Arnoux et al., 2017) indicates the connection between magma flux and hydrothermal discharge. Arnoux et al. (2019) seismically mapped low-velocity volumes and showed elevated percentages of mantle melt in the central part of the segment. Peaks of >10% melt are at ~47°51′N, 47°58′N, and 48°04′N, although these are still far lower percentages of mantle melt than occur in the Endeavour-West Valley and Endeavour-Northern Symmetrical overlapping spreading center zones at the north and south ends of the Endeavour segment, where hydrothermal activity is unknown. These peaks in percent mantle melt extend farther south and north than chimneys occur and so correlate poorly with the distribution of chimneys. The amount of hydrothermal activity does not appear to be directly tied to the total amount of melt in the crust, in the mantle, or in the crust and the mantle (Arnoux et al., 2019). Nor does hydrothermal activity appear related to crustal thickness along the ridge (Arnoux et al., 2019; Soule et al., 2016).

The presence of an AMC therefore appears to be a primary control on the distribution of hydrothermal activity on Endeavour. The presence of off-axis chimneys only in the central 2.8 km of the segment suggests that hydrothermal activity began above a central 2.8-km long AMC about 5,850 years ago (the age of the oldest flank chimney; Jamieson et al., 2013). The central AMC has subsequently extended along the axis and provided the heat to produce chimneys along the axis and now underlies the central ~14 km along axis of the axial graben. The off-axis chimneys are therefore relicts of the initial part of the hydrothermal phase as the AMC was expanding as magma supply increased to end the tectonic phase (Clague et al., 2014). All flank chimneys that have been observed are inactive, and those few that have been dated are between 1,710 to 5,850 years old (Jamieson et al., 2013), in agreement with this explanation.

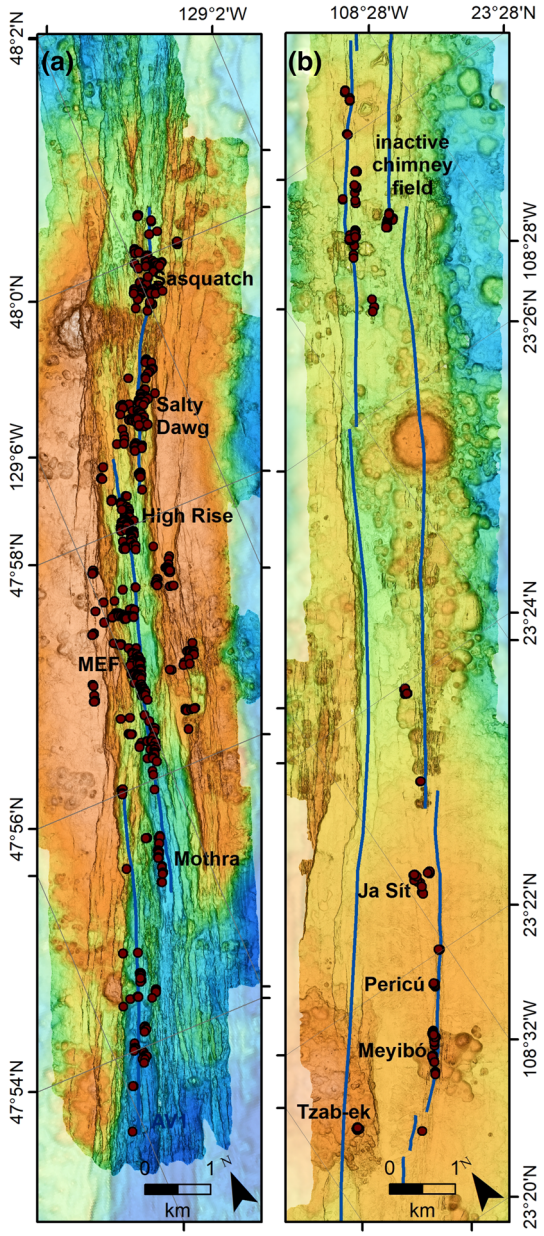

Figure 6. Central Endeavour Segment (a) and Alarcon Rise (b) at same scale showing AUV high-resolution bathymetry from Clague et al. (2014, 2018), segment axes from Le Saout et al. (2019), and chimneys from Figure 2 for Endeavour Rise and Paduan et al. (2018) for Alarcon Rise. Endeavour map projection, rotation from north and depth range as in Figure 2. Alarcon Rise map is in UTM zone 12 N, rotated 33° from north, and has a depth range from −2,650 (dark blue) to −2,150 m (orange). Chimneys on Alarcon are more closely aligned along segment axes (blue lines from Le Saout et al., 2019) and much less abundant than at Endeavour Segment. Parallel subsegment axes at Alarcon Rise indicate recent ridge jumps from the northwest to the southeast. The southernmost mapped chimneys on the two maps are aligned, so chimneys extend along ~3 km more of the Alarcon Rise than along the endeavour segment.

5.2. Why Does Endeavour Have So Many Chimneys?

Many, if not most, segments of the global intermediate to fast spreading ridges have a seismically mapped axial magma lens (e.g., Canales et al., 2012; Carbotte et al., 2012), yet Endeavour appears to be unique in the abundance and size of the chimneys (e.g., Kelley et al., 2013). How unusual is Endeavour in the abundance of chimneys or their size? The Alarcon Rise is the only segment of the mid-ocean ridge system to be entirely mapped at 1-m resolution (Clague et al., 2018; Paduan et al., 2018), like the central portion of Endeavour, and it provides a comparison (Figure 6).

At Alarcon, the AUV mapping revealed 109 chimneys along the central 16 km of the 47-km long segment axis (Paduan et al., 2018). Of these, 31 chimneys were observed to be active, 53 were inactive, and 25 were not observed. The active Tzab-ek field is located about 1 km northwest of the present axis, and the other fields lie on or near the present axis or along pre-ridge jump axes (Le Saout et al., 2019). Chimneys are spread over roughly one third of the segment and occur on and off the present axis, as they do at Endeavour. The number of known active chimneys is about two thirds as many as at Endeavour. There, the active and inactive chimneys occur along 17.5 km of the segment compared with 14.5 km on Endeavour Segment, and the largest chimneys are 31 and 33 m tall (Paduan et al., 2018), compared to the tallest at Endeavour at 27 m (measured from the AUV data), or the 45-m tall Godzilla prior to collapsing (Robigou et al., 1995).

Endeavour may have produced a greater number of chimneys due to high crustal permeability created during a seismically active (Weekly et al., 2013) tectonic phase (Clague et al., 2014). What makes Endeavour so dramatically distinctive, however, is not the number of active chimneys nor their size, but the large number of inactive chimneys. Hydrothermal activity at MEF has persisted for at least 2,300 years and at Sasquatch for at least 1,500 years (Jamieson et al., 2013). The primary reason for this difference is most likely that old, inactive chimneys that formed during the past several thousand years at Alarcon Rise are simply buried beneath the more voluminous and frequent lava flows erupted there (Clague et al., 2018) compared to Endeavour, where minimal volcanic activity has occurred in the past several thousand years (Clague et al., 2014).

The few young flows at Endeavour are small, channelized flows in the axial graben or on the near-graben rims (Clague et al., 2014). As volcanism increases at Endeavour, we can expect that the flows will rapidly bury many of the chimneys, especially considering that most of the chimneys are less than 8 m tall. This analysis supports the three-phase magmatic/tectonic/hydrothermal model proposed by Clague et al. (2014) in which Endeavour is just entering its next magmatic phase, but has yet to overwhelm with lava flows the extinct chimneys located in and near the axial graben. Alarcon Rise, in contrast, has entered a new magmatic phase (Clague et al., 2018) and has already buried most earlier extinct chimneys, if there were any, leaving mainly those that are active or were recently active. Endeavour is unusual simply because it is in the brief period at the end of the tectonic phase prior to more extensive and widespread magmatic activity that will erase most evidence of its current hydrothermal phase.

6. Conclusions

Hydrothermal chimneys and active hydrothermal chimneys are 5 and 1.5 times more abundant, respectively, on Endeavour than they are along a comparable portion of the Alarcon Rise. The abundance of inactive chimneys at Endeavour is what sets the ridge apart from other well-studied ridge segments. The difference and the underlying cause of the high abundance of inactive chimneys at Endeavour Segment is that it has been in a tectonic phase and the next magmatic phase of ridge development began so recently that lava flows have yet to bury the inactive chimneys in the axial graben or on the rims of the graben at Endeavour Segment. Alarcon Rise has advanced into the robust magmatic phase, and lava flows have likely buried chimneys formed during the prior hydrothermal phase.

Acknowledgments
The ABE surveys were collected as part of a joint project between University of Washington, the W. M Keck Foundation, and Neptune Canada. The MBARI AUV data were collected from the R/V *Atlantis* in 2008 and the R/V *Zephyr* in 2011 with the steady hands of ships' captains and crews, and the MBARI AUV team's professionalism responsible for the excellent data obtained. The bathymetric swath data are available at IEDA, and grids and geotiffs are available through the IEDA RIDGE Portal at Lamont Doherty Geological Observatory (10.1594/IEDA/321401, 10.1594/IEDA/321402, 10.1594/IEDA/321403). Marilena Calarco and Melissa Johnson assisted with identifying and measuring the chimneys in the AUV data. The MBARI AUV data collection and processing were supported by a grant to MBARI from the David and Lucile Packard Foundation and by grants from NSF to JH under OCE 0732611, to DAC and DWC under OCE 1043274, and to DSK under OCE 1043403.

References

Arnoux, G. M., Toomey, D. R., Hooft, E. E. E., & Wilcock, W. S. D. (2019). Seismic imaging and physical properties of the Endeavour Segment: Evidence that skew between mantle and crustal magmatic systems governs spreading center processes. *Geochemistry, Geophysics, Geosystems*, *20*, 1319–1339. https://doi.org/10.1029/2018GC007978

Arnoux, G. M., Toomey, D. R., Hooft, E. E. E., Wilcock, W. S. D., Morgan, J., Warner, M., & VanderBeek, B. P. (2017). Seismic evidence that black smoker heat flux is influenced by localized magma replenishment and associated increases in crustal permeability. *Geophysical Research Letters*, *44*, 1687–1695. https://doi.org/10.1002/2016GL071990

Ballard, R. D., Holcomb, R. T., & van Andel, T. H. (1979). The Galapagos rift at 86°W: Part 3. Sheet flows, collapse pits, and lava lakes of the rift valley. *Journal of Geophysical Research*, *84*, 5407–5422. https://doi.org/10.1029/JB084ib10p05407

Barnes, C. R., Best, M. M. R., Pautet, L., & Pirenne, B. (2011). Understanding Earth-Ocean processes using real-time data from NEPTUNE, Canada's widely distributed sensor networks, Northeast Pacific. *Geoscience Canada*, *38*(1), 21–30.

Canales, J. P., Carton, H., Mutter, J. C., Harding, A., Carbotte, S. M., & Nedimovic, M. R. (2012). Recent advances in multichannel seismic imaging for academic research in deep ocean environments. *Oceanography*, *25*(1), 113–115. https://doi.org/10.5670/oceanog.2012.09

Carbotte, S. M., Canales, J. P., Nedimovic, M. R., Carton, H., & Mutter, J. C. (2012). Recent seismic studies of the East Pacific rise 8°20′-10° 10′N and Endeavour segment: Insights into mid-ocean ridge hydrothermal and magmatic processes. *Oceanography*, *25*(1), 100–112. https://doi.org/10.5670/oceanog.2012.08

Caress, D. W., & Chayes, D. N. (1996). Improved processing of Hydrosweep DS multibeam data on the R/V Maurice Ewing. *Marine Geophysical Researches*, *18*, 631–650. https://doi.org/10.1007/BF00313878

Caress, D. W., & Chayes, D. N. (2011). *MB-System: Open source software for the processing and display of swath mapping sonar data*. Palisades, N. Y. (Available at: Lamont-Doherty Earth Obs. of Columbia Univ. http://www.mbari.org/data/mbsystem/

Caress, D. W., Thomas, H., Kirkwood, W. J., McEwen, R., Henthorn, R., Clague, D. A., et al. (2008). High-resolution multibeam, sidescan, and subbottom surveys using the MBARI AUV D. Allan B. In J. R. Reynolds, & H. G. Greene (Eds.), *Marine Habitat Mapping Technology for Alaska*, (pp. 47–69). Fairbanks, Alaska: Alaska Sea Grant Coll. Program, Univ. of Alaska. https://doi.org/10.4027/mhmta.2008.04

Clague, D. A., Caress, D. W., Dreyer, B. M., Lundsten, L., Paduan, J. B., Portner, R. A., et al. (2018). Geology of the Alarcon Rise. *Geochemistry, Geophysics, Geosystems*, *19*(3), 807–837. https://doi.org/10.1002/2017GC007348

Clague, D. A., Caress, D. W., Thomas, H., Thompson, D., Calarco, M., Holden, J., & Butterfield, D. (2008). Abundance and distribution of hydrothermal chimneys and mounds on the Endeavour Ridge determined by 1-m resolution AUV multibeam mapping surveys. *EOS. Transactions of the American Geophysical Union*, *89*(53). Fall Meeting, Supplement Abstract V41B-2079

Clague, D. A., Dreyer, B. M., Paduan, J. B., Martin, J. F., Caress, D. W., Gill, J. B., et al. (2014). Eruptive and tectonic history of the Endeavour segment, Juan de Fuca Ridge, based on AUV mapping data and lava flow ages. *Geochemistry, Geophysics, Geosystems*, *15*(8), 3364–3391. https://doi.org/10.1002/2014gc005415

Clague, D. A., & Paduan, J. B. (2009). Submarine basaltic volcanism. In B. Cousens, & S. J. Piercey (Eds.), *Submarine volcanism and mineralization—Modern through ancient*. Geological Association of Canada. Short Course 29–30 May 2008, Quebec City, Canada, 41–60, with color plates 157–165

Delaney, J. R., Kelley, D. S., Lilley, M. D., Butterfield, D. A., McDuff, R. E., Baross, J. A., et al. (1997). The Endeavour hydrothermal system I: Cellular circulation above an active cracking front yields large sulfide structures, "fresh" vent water and hyperthermophilic Archaea. *RIDGE Events*, *8*(2), 11–19.

Delaney, J. R., Robigou, V., & McDuff, R. (1992). Geology of a vigorous hydrothermal system on the Endeavour Segment, Juan de Fuca Ridge. *Journal of Geophysical Research*, *97*, 19,663–19,682. https://doi.org/10.1029/92JB00174

DeMets, C., Gordon, R. G., & Argus, D. F. (2010). Geologically current plate motions. *Geophysical Journal International*, *181*(1), 1–80. https://doi.org/10.1111/j.1365-246x.2009.04491.x

Fundis, A. T., Soule, S. A., Fornari, D. J., & Perfit, M. R. (2010). Paving the seafloor: Volcanic emplacement processes during the 2005-2006 eruptions at the fast-spreading East Pacific Rise, 9°50′N. *Geochemistry, Geophysics, Geosystems*, *11*, Q08024. https://doi.org/10.1029/2010GC003058

Glickson, D. A., Kelley, D. S., & Delaney, J. R. (2006). The Sasquatch Hydrothermal Field: Linkages between seismic activity, hydrothermal flow, and geology. *EOS. Transactions of the American Geophysical Union*, *87*(52). Fall Meeting Supplement Abstract V23B-0614

Glickson, D. A., Kelley, D. S., & Delaney, J. R. (2007). Geology and hydrothermal evolution of the Mothra hydrothermal field, Endeavour Segment, Juan de Fuca Ridge. *Geochemistry, Geophysics, Geosystems*, *8*, Q06010. https://doi.org/10.1029/2007GC001588

Hooft, E. E. E., Patel, H., Wilcock, W. S. D., Becker, K., Butterfield, D., Davis, E., et al. (2010). A seismic swarm and regional hydrothermal and hydrologic perturbations: The northern Endeavour Segment, 2005. *Geochemistry, Geophysics, Geosystems*, *11*, Q12015. https://doi.org/10.1029/2010GC003264

Jamieson, J. W., Clague, D. A., & Hannington, M. D. (2014). Hydrothermal sulfide accumulation along the Endeavour Segment, Juan de Fuca Ridge. *Earth and Planetary Science Letters*, *395*, 136–148. https://doi.org/10.1016/J.epsl.2014.03.035

Jamieson, J. W., Hannington, M. D., Clague, D. A., Kelley, D. S., Holden, J. S., Tivey, M. K., & Kimpe, L. E. (2013). History of hydrothermal venting along the Endeavour Segment of the Juan de Fuca Ridge. *Geochemistry, Geophysics, Geosystems*, *14*, 2084–2099. https://doi.org/10.1002/ggge.20133

Kappel, E. S., & Ryan, W. B. F. (1986). Volcanic episodicity and a non-steady state rift valley along the Northeast Pacific spreading centers: Evidence from sea MARC I. *Journal of Geophysical Research*, *91*, 13,925–13,940. https://doi.org/10.1029/JB091iB14p13925

Karsten, J., Hammond, S. R., Davis, E. E., & Currie, R. G. (1986). Detailed geomorphology and neotectonics of the Endeavour Segment, Juan de Fuca Ridge: New results from Seabeam swath mapping. *Geological Society of America Bulletin*, *97*, 213–221. https://doi.org/10.1130/0016-7606

Karsten, J. L., Delaney, J. R., Rhodes, J. M., & Liias, R. A. (1990). Spatial and temporal evolution of magmatic systems beneath the Endeavour segment, Juan de Fuca ridge: Tectonic and petrologic constraints. *Journal of Geophysical Research*, *95*, 19,235–19,256. https://doi.org/10.1029/JB095iB12p19235

Kelley, D. S., Baross, J. A., & Delaney, J. R. (2002). Volcanoes, fluids, and life in submarine environments. *Annual Review of Earth and Planetary Sciences*, *30*, 385–491. https://doi.org/10.1146/annurev.earth.30.091201.141331

Kelley, D. S., Carbotte, S. M., Caress, D. W., Clague, D. A., Delaney, J. R., Gill, J. B., et al. (2012). Endeavour segment of the Juan de Fuca ridge: One of the most remarkable places on earth. *Oceanography*, *25*(1), 44–61. https://doi.org/10.5670/oceanog.2012.03

Kelley, D. S., Delaney, J. R., & Juniper, S. K. (2014). Establishing a new era of submarine volcanic observatories: Cabling axial seamount and the Endeavour Segment of the Juan de Fuca Ridge. *Marine Geology*, *352*, 426–450. https://doi.org/10.1016/j.margeo.2014.03.010

Kelley, D. S., Delaney, J. R., & Yoerger, D. A. (2001). Geology and venting characteristics of the Mothra hydrothermal field, Endeavour Segment, Juan de Fuca Ridge. *Geology*, *29*, 959–962. https://doi.org/10.1130/0091-7613(2001)029<0959:gavcot>2.0.co;2

Le Saout, M., Clague, D. A., & Paduan, J. B. (2019). Evolution of fine-scale segmentation at intermediate-spreading ridges. *Geochemistry, Geophysics, Geosystems*, *20*, 3841-3860. https://doi.org/10.1029/2019GC008218

Lilley, M. D., Butterfield, D. A., Lupton, J. E., & Olson, E. J. (2003). Magmatic events can produce rapid changes in hydrothermal vent chemistry. *Nature*, *422*(6934), 878–881. https://doi.org/10.1038/nature01569

Paduan, J. B., Caress, D. W., Clague, D. A., Paull, C. K., & Thomas, H. (2009). High-resolution mapping of erosional, tectonic, and volcanic hazards using the MBARI mapping AUV. *Rendiconti Online della Società Geologica Italiana*, *7*, 181–186.

Paduan, J. B., Zierenberg, R. A., Clague, D. A., Caress, D. W., Thomas, H., Troni, G., et al. (2018). Hydrothermal vent fields on Alarcon Rise and in the southern Pescadero Basin, southern Gulf of California. *Geochemistry, Geophysics, Geosystems*, *19*, 4788-4819. https://doi.org/10.1029/2018GC007771

Perfit, M. R., & Chadwick, W. W. Jr. (1998). Magmatism at mid-ocean ridges: Constraints from volcanological and geochemical investigations. In W. R. Buck, P. T. Delaney, J. A. Karson, & Y. Lagabrielle (Eds.), *Faulting and magmatism at mid-ocean ridges*, *Geophysical Monograph Series*, (Vol. 106, pp. 59–115). Washington, DC: Am. Geophys. Union.

Robigou, V., Delaney, J. R., & Parker, C. B. (1995). Rapid growth of sulfide deposits in hydrothermal vent fields of the Endeavour Segment, Juan de Fuca Ridge. *EOS. Transactions of the American Geophysical Union*, *76*, 420.

Robigou, V. R., Delaney, J. R., & Stakes, D. S. (1993). Large massive sulfide deposits in a newly discovered active hydrothermal system, the High Rise Field, Endeavour Segment, Juan de Fuca Ridge. *Geophysical Research Letters*, *20*, 1887–1890. https://doi.org/10.1029/93GL01399

Soule, D., Wilcock, W. S. D., Toomey, R. R., Hooft, E. E. E., & Weekly, R. T. (2016). Near-axis crustal structure and thickness of the Endeavour Segment, Juan De Fuca Ridge. *Geophysical Research Letters*, *43*, 5688-5695. https://doi.org/10.1002/2016GL068182

Van Ark, E. M., Detrick, R. S., Canales, J. P., Carbotte, S. M., Haring, A. J., Kent, G. M., et al. (2007). Seismic structure of the Endeavour Segment, Juan de Fuca Ridge: Correlations with seismicity and hydrothermal activity. *Journal of Geophysical Research*, *112*, B02401. https://doi.org/10.1029/2005JB004210

VanderBeek, B. P., Toomey, D. R., Hooft, E. E. E., & Wilcock, W. S. D. (2016). Segmentation of mid-ocean ridges attributed to oblique mantle divergence. *Nature Geoscience*, *9*(8), 636–642. https://doi.org/10.1038/NGEO2745

Weekly, R. T., Wilcock, W. S. D., Hooft, E. E. E., Toomey, D. R., McGill, P. R., & Stakes, D. S. (2013). Termination of a 6 year ridge spreading event observed using a seafloor seismic network on the Endeavour Segment, Juan de Fuca Ridge. *Geochemistry, Geophysics, Geosystems*, *14*. https://doi.org/10.1002/ggge.20105